inorganics

MDPI

Supporting Information

High-Coercivity Ferrimagnet $Co_2FeO_2BO_3$: XMCD Insights into Charge-Ordering and Cation Distribution

Mikhail S. Platunov

Synchrotron Radiation Facility SKIF, 630559 Kol'tsovo, Russia; m.s.platunov@srf-skif.ru

Abstract: The multi-sublattice ferrimagnet $Co_2FeO_2BO_3$, a prominent example of lanthanide-free magnets, was the subject of element-selective studies using X-ray magnetic circular dichroism (XMCD) observations at the *L*- and *K*- X-ray absorption edges. Research findings indicate that the distinct magnetic characteristics of $Co_2FeO_2BO_3$, namely its remarkable high coercivity (which surpasses 7 Tesla at low temperatures), originate from an atypical arrangement of magnetic ions in the crystal structure (sp.gr. *Pbam*). The antiferromagnetic nature of the Co^{2+}-O-Fe^{3+} exchange interaction was confirmed by identifying the spin and orbital contributions to the total magnetization from Co (m_L = 0.27 ± 0.1 μ_B/ion and m^{eff}_S = 0.53 ± 0.1 μ_B/ion) and Fe (m_L = 0.05 ± 0.1 μ_B/ion and m^{eff}_S = 0.80 ± 0.1 μ_B/ion) ions through element-selective XMCD analysis. Additionally, the research explicitly revealed that the strong magnetic anisotropy is a result of the significant unquenched orbital magnetic moment of Co, a feature that is also present in the related compound $Co_3O_2BO_3$. A complex magnetic structure in $Co_2FeO_2BO_3$, with infinite $Co^{2+}O_6$ layers in the **bc**-plane and strong antiferromagnetic coupling through Fe^{3+} ions, is suggested by element-selective hysteresis data, which revealed that Co^{2+} ions contribute both antiferromagnetic and ferromagnetic components to the total magnetization. The findings underline the suitability of $Co_2FeO_2BO_3$ for applications in extreme environments, such as low temperatures and high magnetic fields, where its unique magnetic topology and anisotropy can be harnessed for advanced technologies, including materials for space exploration and quantum devices. This XMCD study opens the door to the production of novel high-coercivity, lanthanide-free magnetic materials by showing that targeted substitution at specific crystallographic sites can significantly enhance the magnetic properties of such materials.

Keywords: magnetism; coercive field; element-specificity; orbital-specificity; charge ordering

TOC Image

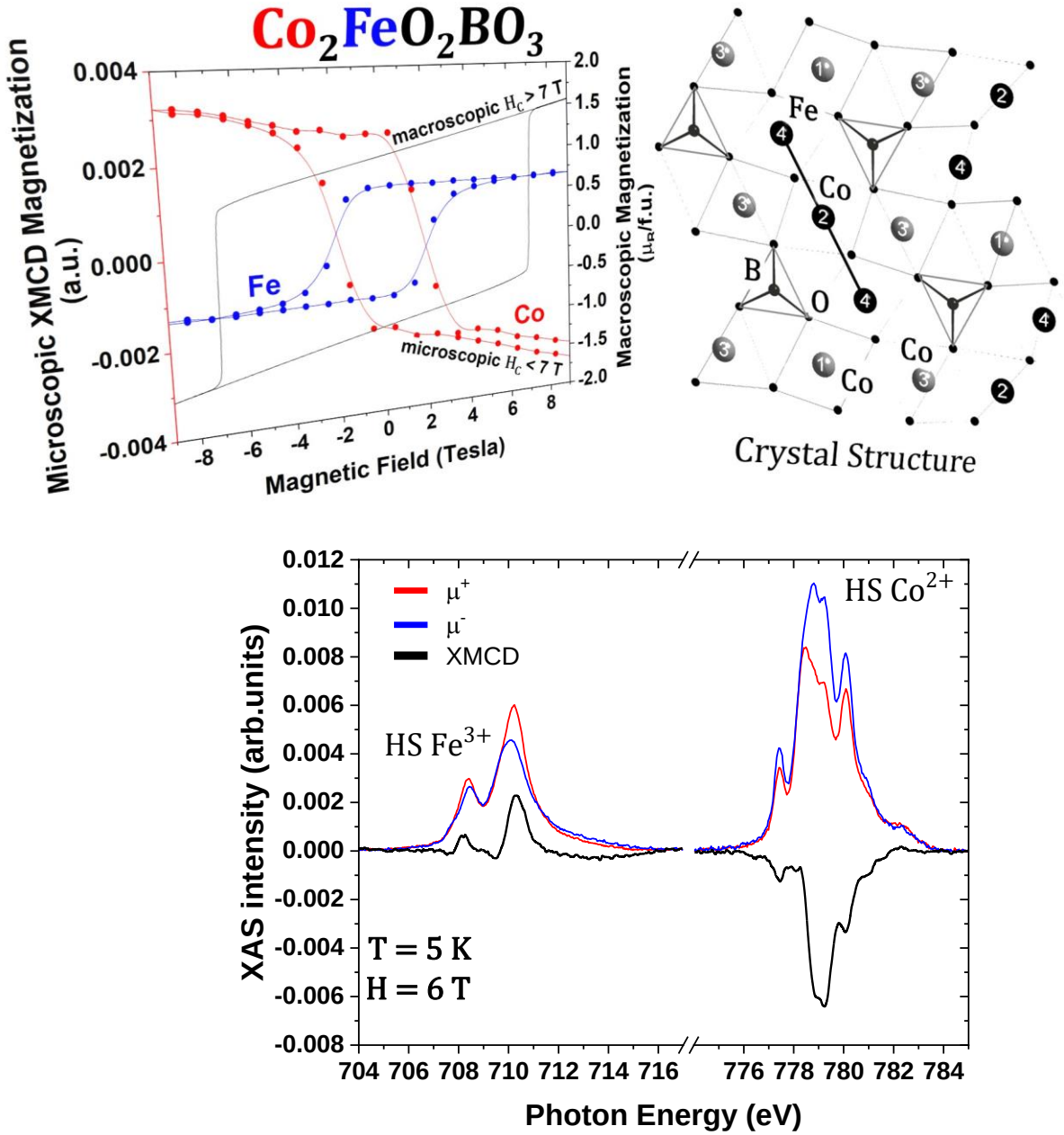

Figure S1. XAS spectra for left and right polarizations of the X-ray beam and the corresponding XMCD spectra for the $Co_2FeO_2BO_3$ crystal, measured at the L_3-edges of Co *(a)* and Fe *(b)*, recorded at 5 K in a magnetic field of 6 T.

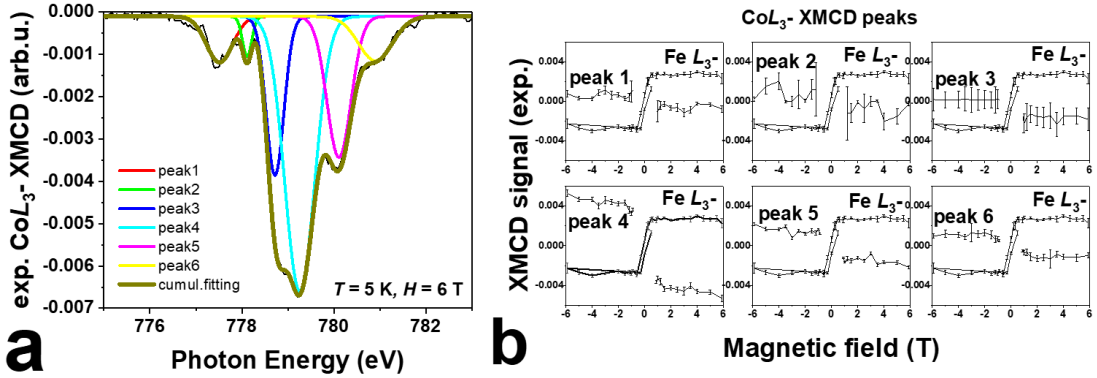

Figure S2. *(a)* Experimental XMCD signal at the Co L_3-edge of the $Co_2FeO_2BO_3$ sample at 5 K and 6 T, decomposed into six Gaussian peaks. *(b)* Magnetic field dependence of these six XMCD peaks measured at the L_3-edge of cobalt, likely corresponding to different magnetic sublattices. For comparison, an element-selective curve measured at the L_3-edge of iron is also included. Peaks 4 and 5 show a sloped dependence in the XMCD signal for cobalt, suggesting they are linked to sublattices with an antiferromagnetic component. Peaks 1, 2, 3, and 6 exhibit saturation behavior, likely associated with Co^{2+} in crystallographic sites that compensate for the magnetic moments of iron.

Figure S2 displays the experimental XMCD signal at the Co L_3-edge of the $Co_2FeO_2BO_3$ sample measured at 5 K and 6 T. The signal is decomposed into six Gaussian peaks, each representing distinct contributions to the overall magnetization. Figure S2*(b)* illustrates the magnetic field dependence of these six XMCD signal peaks at the L_3-edge of cobalt, suggesting correspondence to magnetic sublattices with both ferromagnetic and antiferromagnetic components. For comparison, the XMCD signal of iron shows only two peaks in its asymptotic field dependence, each of which have the same behavior. An element-selective curve at the L_3-edge of iron is also provided for context.

Notably, peaks 4 and 5 in the cobalt XMCD signal demonstrate a sloped field dependence, indicating a potential connection to sublattices with an antiferromagnetic component. In contrast, peaks 1, 2, 3, and 6 exhibit saturation behavior, which is likely attributable to Co^{2+} ions in crystallographic sites that compensate for the magnetic moments of iron. This detailed analysis of the XMCD signal and its decomposition into Gaussian peaks enhances our understanding of the complex magnetic interactions in $Co_2FeO_2BO_3$. It underscores the importance of considering both element- and sublattice-selective contributions to the overall magnetic properties of such materials.

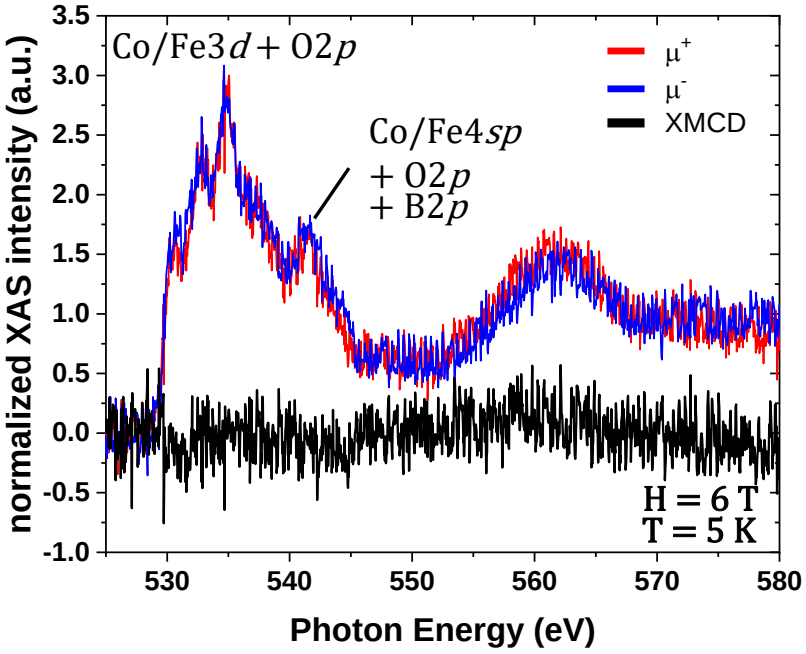

Figure S3. Experimental XAS spectrum of the O-*K* edge measured along the **b**-axis.

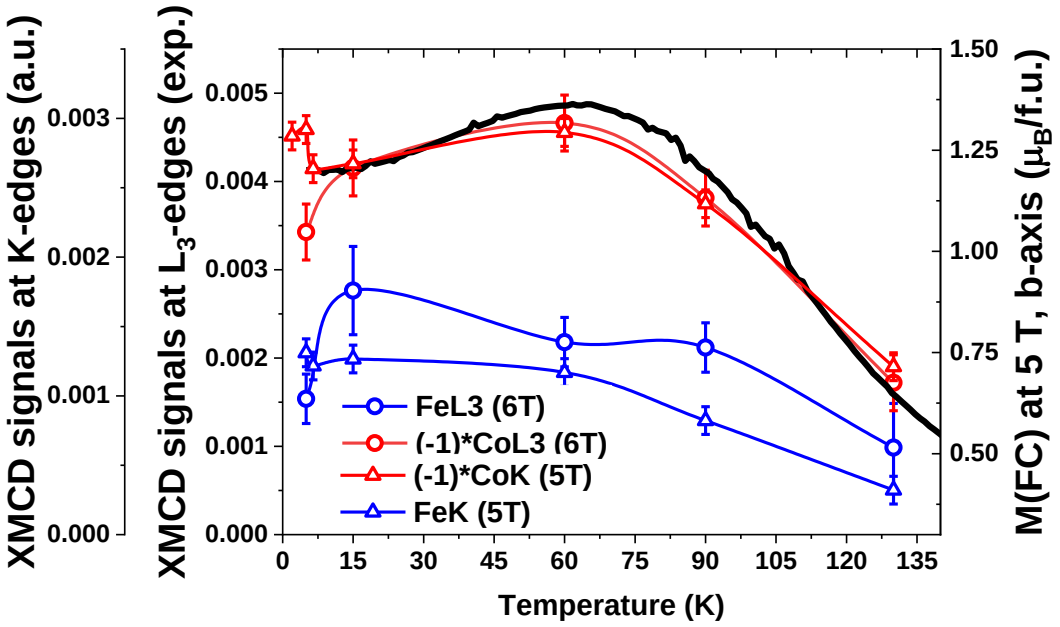

Figure S4. Temperature-dependent field-cooled magnetization curve for $Co_2FeO_2BO_3$ under a 0.1 T magnetic field, compared with element-selective magnetization curves for the Co and Fe sublattices measured along the **b**-axis under the same conditions. The |Co*K*-Fe*K*| signal difference is plotted for visual comparison, assuming that the integrated XMCD signals for cobalt and iron near the 1s-(3d-4p) transitions are comparable. This comparison suggests strong interactions and simultaneous magnetic ordering of the sublattices across the entire temperature range, contradicting previous studies on similar bicomponent compounds such as $Co_2FeO_2BO_3$ [1], $Ni_2FeO_2BO_3$ [2,3], $Cu_2FeO_2BO_3$ [4,5], and $Fe_3O_2BO_3$ [6,7].

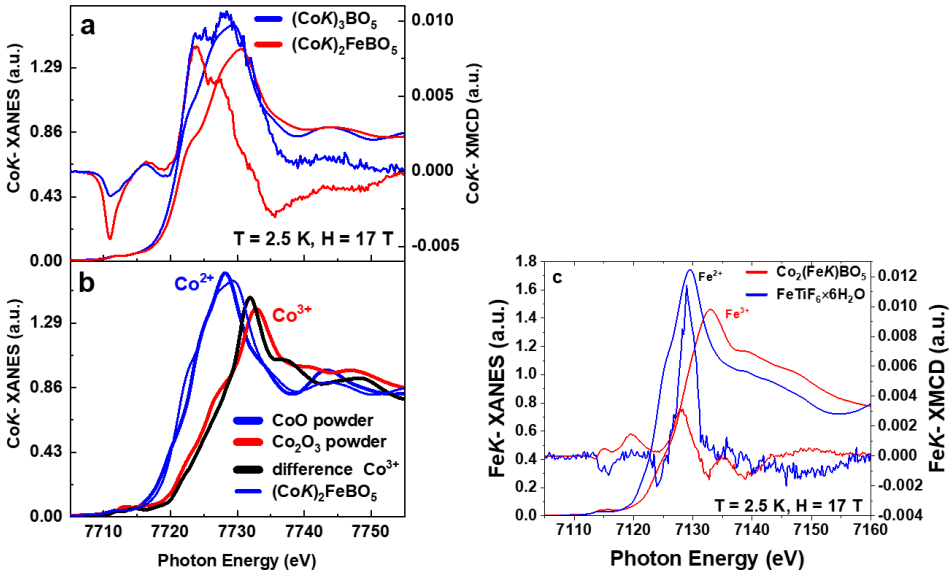

Figure S5. *(a)* Normalized Co *K*-edge XANES and XMCD spectra recorded at T = 5 K in a 17 T magnetic field for $Co_3O_2BO_3$ and $Co_2FeO_2BO_3$ single crystals. *(b)* Comparison of the XANES spectra of $Co_2FeO_2BO_3$ with the difference spectrum (3 × $Co_3O_2BO_3$ – 2 × $Co_2FeO_2BO_3$) and the spectra of Co_2O_3 and CoO standards at room temperature. The difference spectrum corresponds to the charge state of the Co^{3+} ion, while the cobalt ions in $Co_2FeO_2BO_3$ correspond to the 2+ charge state. Minor differences are attributed to variations in the fine electronic structure. *(c)* Comparison of normalized XMCD and XANES spectra near the iron *K*-edge for $Co_2Fe(HS\ 3+)O_2BO_3$ and for $Fe(HS\ 2+)TiF_6$ (digitized from [8]) samples, measured at 2.5 K under H = 17 T.

Figure S5 illustrates the application of the proposed experimental spectroscopic technique, which allows for the investigation of magnetic contributions from ions of the same element but with different charge states within multicomponent magnetic compounds that have complex crystal structures. The effectiveness of this method is demonstrated using the single crystal $Co_3O_2BO_3$, which contains both Co^{2+} and Co^{3+} ions [see also reference 25 in the main manuscript]. This is achieved by measuring the XANES and XMCD spectra at the Co *K*-edge at low temperatures (at T = 5 K) and under strong magnetic fields (up to H = ±17 T), and comparing these spectra with those of the isostructural compound $Co_2FeO_2BO_3$. This approach requires that measurements for the two isostructural materials be performed under identical temperature and field conditions along the same crystallographic axis.

Performing these experiments necessitates not only meticulous data analysis but also careful execution of XMCD experiments, with strict control over the focal spot size of the X-ray beam, ideally using X-ray optics elements. Furthermore, these experiments should be carried out under ultrahigh vacuum conditions, with the appropriate selection of detection devices (energy-resolved, avalanche photodiodes in backscattering geometry etc.). The methodology, based on the measurement of X-ray absorption spectra near the *K*-edge of cobalt, is described in detail below.

The conclusions about the magnetic state of $Co_3O_2BO_3$ [9] were confirmed by direct neutron diffraction measurements of the magnetic structure [10]. According to [10], at T = 4.2 K, Co^{2+} ions have magnetic moments typical of the high-spin (HS) state: 3.6 μ_B (site 1), 3.1 μ_B (site 2), 3.8 μ_B (site 3), and a strongly suppressed moment of 0.5 μ_B for the Co^{3+} ion (site 4). All moments lie within the **ab**-plane, with a preferential orientation along the **b**-axis. The spin configuration 1(↓)2(↑)3(↑)4(↓), where arrows denote the up and down spin direction, yields an uncompensated magnetic moment of approximately 3.11 μ_B/f.u. As a result, the ground magnetic state of $Co_3O_2BO_3$ was determined to be ferrimagnetic. The

small magnetic moment observed at site 4 is attributed to the low-spin (LS) state of the Co^{3+} ions.

$Co_2FeO_2BO_3$ is an isostructural analog of cobalt ludwigite, where Fe^{3+} ions substitute Co^{3+} ions at the crystallographic site 4, maintaining the ferrimagnetic spin order and magnetic anisotropy.

XMCD measurements were performed at the Co *K*-edge, typically under low temperatures and high magnetic fields to ensure magnetic saturation. XMCD near the *K*-edge explores transitions from 1s to empty 4p states, while the pre-edge feature (between 7710 and 7715 eV in Fig. S5*(a)*) is associated with transitions to more localized unoccupied 3d states arising from Co 4p-3d hybridization. XANES and XMCD spectra at the Co *K*-edge in $Co_3O_2BO_3$ and $Co_2FeO_2BO_3$ were measured at low temperatures (T = 5 K) and in a strong magnetic field (H = ±17 T) aligned parallel to the **b-**axis. Figures S5*(a,b)* show Co *K*-edge XANES spectra characterized by a sharp pre-edge peak at 7710 eV and a main peak at 7730 eV. A comparison of the normalized Co *K*-edge XANES spectra at room temperature for $Co_3O_2BO_3$, $Co_2FeO_2BO_3$, CoO, and Co_2O_3 reveals distinct differences attributable to the Co^{2+} and Co^{3+} charged states.

The clear and non-zero XMCD signal in the pre *K*-edge region for both samples reflects the magnetic polarization of the Co 4p band due to intraatomic exchange interactions with the 3d band. The negative sign of this XMCD signal shows that in both crystals, the magnetization of the Co sublattice is parallel to the applied magnetic field (Fig. S5). Within the framework of the additivity model, the ratio of these signals can be expressed as $\frac{\mathrm{XMCD(Co2Co)}}{\mathrm{XMCD(Co2Fe)}} = \frac{2}{3} \cdot \left(1 + \frac{\mathrm{XMCD_{Co^{3+}}}}{2 \cdot \mathrm{XMCD_{Co^{2+}}}}\right)$, where $\mathrm{XMCD_{Co^{2+}}}$ and $\mathrm{XMCD_{Co^{3+}}}$ represent the contributions of the divalent and trivalent subsystems to the integrated XMCD pre *K*-edge signal, respectively.

As Co^{3+} is replaced by Fe^{3+}, the XMCD signal at the pre-edge, reflecting the magnetic polarization of the Co 4p band, increases, suggesting a negligible net magnetization from Co^{3+} ions. This observation supports the hypothesis [10] that Co^{3+} ions in $Co_3O_2BO_3$ do not significantly contribute to the magnetic properties. The additive model used to interpret the XMCD data implies that Co^{2+} ions predominantly determine the magnetism in ludwigite, with the influence of Co^{3+} ions being suppressed in $Co_3O_2BO_3$ compared to $Co_2FeO_2BO_3$.

Given that $Co_3O_2BO_3$ contains both Co^{2+} and Co^{3+} ions, while $Co_2FeO_2BO_3$ contains only Co^{2+} ions, the expected XMCD signal ratio, assuming Co^{3+} ions are in the LS state (contributing minimally to magnetization), should be approximately 0.66. Integration of the XMCD spectra at the Co *K*-edges for both compounds in the region of the quadrupole 1s-3d transition yields a ratio of 0.69. This slight discrepancy suggests a minimal but non-zero magnetic contribution from Co^{3+} ions, reinforcing that these ions are in the LS state with negligible unpaired spins ($t_{2g}^6 e_g^0$, $S = 0$).

Figure S5*(b)* compares the XANES spectra for $Co_2FeO_2BO_3$ with CoO(Co^{2+}) and Co_2O_3 (Co^{3+}) standards, indicating that $Co_2FeO_2BO_3$ primarily contains only Co^{2+} ion. The difference between $Co_3O_2BO_3$ and $Co_2FeO_2BO_3$ relative to the Co^{3+} standard further confirms the presence of Co^{3+} ions in $Co_3O_2BO_3$. This comparison provides evidence that the difference between the two samples is due to the presence of Co^{3+}.

Additionally, Figure S5*(c)* illustrates the difference between $Co_2FeO_2BO_3$ (Fe^{3+}) and a recently published $FeTiF_6$ standard, where iron is shown to exist only in the HS Fe^{2+} state [8]. Therefore, in our $Co_2FeO_2BO_3$ sample, Fe^{3+} is in the high-spin state, and the XMCD sign is opposite to the applied magnetic field.

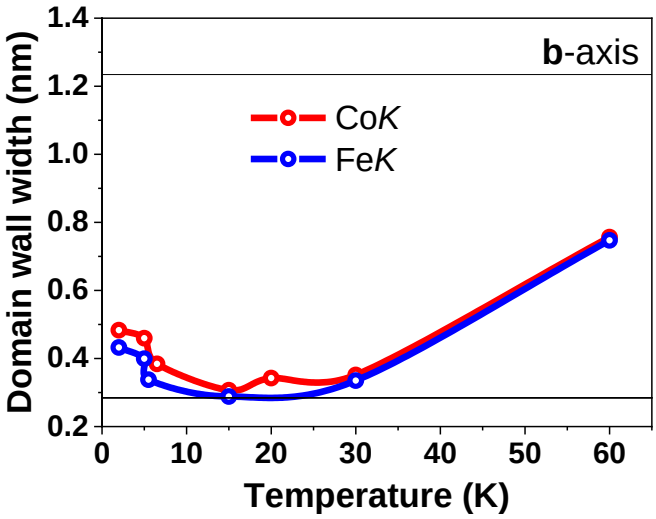

Figure S6. Temperature dependence of the domain wall widths in $Co_2FeO_2BO_3$.

References

1. D.C. Freitas, M.A. Continentino, R.B. Guimaraes, J.C. Fernandes, E.P. Oliveira, R.E. Santelli, J. Ellena, G.G. Eslava, L. Ghivelder, Partial magnetic ordering and crystal structure of the ludwigites $Co_2FeO_2BO_3$ and $Ni_2FeO_2BO_3$, Phys. Rev. B 79(13) (2009) 134437. https://doi.org/10.1103/PhysRevB.79.134437.
2. J.C. Fernandes, R.B. Guimarães, M.A. Continentino, H.A. Borges, A. Sulpice, J.L. Tholence, J.L. Siqueira, J.B.M. Da Cunha, C.A. Dos Santos, Magnetic interactions in the ludwigite $Ni_2FeO_2BO_3$, Phys. Rev. B 58(1) (1998) 287. https://doi.org/10.1103/PhysRevB.58.287.
3. D.A. Perkins, J.P. Attfield, Resonant powder X-ray determination of the cation distribution in $FeNi_2BO_5$, J. Chem. Soc., Chem. Commun. 4 (1991) 229–231. https://doi.org/10.1039/C39910000229.
4. M.A. Continentino, J.C. Fernandes, R.B. Guimarães, H.A. Borges, A. Sulpice, J.-L. Tholence, J.L. Siqueira, J.B.M. Da Cunha, C.A. Dos Santos, Magnetic interactions in the monoclinic ludwigite $Cu_2FeO_2BO_3$, Eur. Phys. J. B 9 (1999) 613–618. https://doi.org/10.1007/s100510050805.
5. G.A. Petrakovskiĭ, L.N. Bezmaternykh, D.A. Velikanov, A.M. Vorotynov, O.A. Bayukov, M. Schneider, Magnetic properties of single crystals of ludwigites Cu_2MBO_5 (M = Fe^{3+}, Ga^{3+}), Phys. Solid State 51 (2009) 2077–2083. https://doi.org/10.1134/S106378340910014X.
6. A.P. Douvalis, A. Moukarika, T. Bakas, G. Kallias, V. Papaefthymiou, Mössbauer and magnetization studies of Fe_3BO_5, J. Phys.: Condens. Matter 14(12) (2002) 3303. https://doi.org/10.1088/0953-8984/14/12/317.
7. P. Bordet, E. Suard, Magnetic structure and charge ordering in Fe_3BO_5: A single-crystal x-ray and neutron powder diffraction study, Phys. Rev. B 79(14) (2009) 144408. https://doi.org/10.1103/PhysRevB.79.144408.
8. M.S. Platunov, N.A. Fedorova, Y.V. Pyastolova, N.M. Laptash, Y.V. Knyazev, F.N. Tomilin, A.A. Dubrovskiy, Unraveling Dynamic Jahn-Teller Effect and Magnetism in $FeTiF_6 \times 6H_2O$ Single Crystal, J. Alloys Compd. (2024) 175104. https://doi.org/10.1016/j.jallcom.2024.175104.
9. J. Bartolomé, A. Arauzo, N.V. Kazak, N.B. Ivanova, S.G. Ovchinnikov, Y.V. Knyazev, I.S. Lyubutin, Uniaxial magnetic anisotropy in $Co_{2.25}Fe_{0.75}O_2BO_3$ compared to $Co_3O_2BO_3$ and $Fe_3O_2BO_3$ ludwigites, Phys. Rev. B 83(14) (2011) 144426. https://doi.org/10.1103/PhysRevB.83.144426.
10. D.C. Freitas, C.P.C. Medrano, D.R. Sanchez, M. Nunez Regueiro, J.A. Rodríguez-Velamazán, M.A. Continentino, Magnetism and charge order in the ladder compound $Co_3O_2BO_3$, Phys. Rev. B 94(17) (2016) 174409. https://doi.org/10.1103/PhysRevB.94.174409.